

# First evidence of a stripped star cluster from the Small Magellanic Cloud

Andrés E. Piatti<sup>1,2\*</sup> and Scott Lucchini<sup>3</sup>

<sup>1</sup>*Instituto Interdisciplinario de Ciencias Básicas (ICB), CONICET-UNCUYO, Padre J. Contreras 1300, M5502JMA, Mendoza, Argentina*

<sup>2</sup>*Consejo Nacional de Investigaciones Científicas y Técnicas, Godoy Cruz 2290, C1425FQB, Buenos Aires, Argentina*

<sup>3</sup>*Department of Physics, University of Wisconsin–Madison, Madison, WI, USA*

Accepted XXX. Received YYY; in original form ZZZ

## ABSTRACT

We present results on the recently discovered stellar system YMCA-1, for which physical nature and belonging to any of the Magellanic System galaxies have been irresolutely analyzed. We used SMASH and *Gaia* EDR3 data sets to conclude that we are dealing with a small star cluster. Its reddening free, field star decontaminated colour-magnitude diagram was explored in order to obtain the cluster parameters. We found that YMCA-1 is a small (435 M<sub>⊙</sub>), moderately old (age = 9.6 Gyr), moderately metal-poor ([Fe/H] = -1.16 dex) star cluster, located at a nearly Small Magellanic Cloud (SMC) distance (60.9 kpc) from the Sun, at ~ 17.1 kpc to the East from the Large Magellanic Cloud (LMC) centre. The derived cluster brightness and size would seem to suggest some resemblance to the recently discovered faint star clusters in the Milky Way (MW) outer halo, although it does not match their age-metallicity relationship, nor those of MW globular clusters formed in-situ or ex-situ, nor that of LMC clusters either, but is in agreement with that of SMC old star clusters. We performed numerical Monte Carlo simulations integrating its orbital motion backward in the MW-LMC-SMC system with radially extended dark matter haloes that experience dynamical friction, and by exploring different radial velocity (RV) regimes for YMCA-1. For RVs ≳ 300 km/s, the cluster remains bound to the LMC during the last 500 Myrs. The detailed tracked kinematic of YMCA-1 suggests that its could have been stripped by the LMC from the SMC during any of the close interactions between both galaxies, a scenario previously predicted by numerical simulations.

**Key words:** galaxies: Magellanic Clouds – galaxies: star cluster

## 1 INTRODUCTION

The search for old star clusters in the outskirts of the Large Magellanic Cloud (LMC) has long been motivated by the fact that they have been thought to be key to reconstructing the early galaxy formation and chemical enrichment history (Geisler et al. 1997). As far as we are aware, a handful of faint star clusters (DES 4, DES 5, Torrealba I, *Gaia* 3) have been recently discovered (Torrealba et al. 2019; Bica et al. 2020, and references therein), in addition to other three stellar systems of uncertain nature, namely, SMASH 1 (Martin et al. 2016), DELVE 2 (Cerny et al. 2021), and YMCA-1 (Gatto et al. 2021). They are stellar aggregates that can be either ultra-faint dwarf galaxies or old star clusters. There are others ~ 22 objects discovered to date in the outskirts of the Magellanic Cloud galaxies that resulted to be ultra-faint dwarf galaxies.

According to (Martin et al. 2016), SMASH-1 could be an ancient, very elongated, star cluster that is being tidally disrupted by the LMC at a distance of ~13 kpc from it. They suggested that the stellar system could have been stripped from the SMC, based on the simulations by (Carpintero et al. 2013). Nevertheless, among the known LMC globular clusters, NGC 1841 tightly matches the age and metallicity of SMASH 1. The former is located at a deprojected distance of 14.25 kpc from the LMC centre, toward the same southern LMC region where SMASH 1 is located, and shows an LMC disk kinematics (Piatti et al. 2019a). This suggests that SMASH 1 could be a member of the LMC globular cluster population. DELVE 2 is located at 28 kpc from the LMC toward the Small Magellanic Cloud (SMC) and, as opposed to SMASH 1, is a nearly spherical very old stellar system. However, simulations of the accreted satellite population of the LMC led Cerny et al. (2021) to conclude that it is very likely associated with the LMC.

\* E-mail: andres.piatti@unc.edu.ar

YMCA-1 has been suggested to be a remote Milky Way

(MW) halo star cluster located at 100 kpc from the Galactic centre. In the sky, it is projected  $\sim 13^\circ$  to the East of the LMC centre. However, [Gatto et al. \(2021\)](#) pointed out that the stellar system nature and the object distance need to be confirmed from deeper photometry. Precisely, the main aim of this work is to take advantage of the SMASH database (obtained similarly as that by the DELVE's team; [Drlica-Wagner et al. \(2021\)](#)) to revisit YMCA-1, in order to estimate accurate astrophysical properties and to uncover its origin. In Section 2 we make use of the available SMASH data sets to estimate YMCA-1's distance, age, metallicity and present mass, and to derive its projected half-light radius from its surface density profile. Section 3 discusses the resulting fundamental parameters to conclude on the stellar system nature and its origin.

## 2 DATA HANDLING

Among the public surveys that cover the Magellanic System, the Survey of the MAGellanic Stellar History (SMASH, [Nidever et al. 2021](#)) is a suitable one for our purposes. Its limiting magnitude is beyond the 25th magnitude in the outskirts of the Magellanic Clouds, which is  $\sim 1.5$  mag underneath the YMCA-1 turnoff (see Fig. 1 in [Gatto et al. 2021](#)). We retrieved data from the Astro Data Lab<sup>1</sup>, which is part of the Community Science and Data Center at NSF's National Optical Infrared Astronomy Research Laboratory. They consist of R.A and Dec. coordinates, PSF  $g, i$  magnitudes and their respective errors,  $E(B-V)$  interstellar reddening and  $\chi$  and SHARPNESS parameters of stellar sources located inside a radius of  $5'$  from the YMCA-1's centre. According to [Gatto et al. \(2021\)](#), the object has a radius of  $0.3'$ . We selected those sources with  $0.2 \leq \text{SHARPNESS} \leq 1.0$  and  $\chi^2 < 0.5$ , in order to exclude bad pixels, cosmic rays, galaxies, and unrecognized double stars. The photometric performance is as mentioned in [Nidever et al. \(2017\)](#). In their Table 4, they presented the SMASH average photometric transformation equations. We added in quadrature zero-point, extinction and colour term errors, and computed an accuracy  $\lesssim 0.02$  mag in  $gi$ . They showed that these calibration errors imply a SMASH photometry precision of  $\sim 0.5$ - $0.7$  per cent in  $gi$ . Such a precision implies in turn an uncertainty of  $\sim 0.12$ - $0.17$  mag in  $gi$ , for a star at  $g \gtrsim 25.0$  mag.

Aiming at disentangling the true nature of YMCA-1, its observed colour-magnitude diagram (CMD) needs to be cleaned from field star contamination. The contamination of field stars plays an important role, because it is not straightforward to consider a star as a member of the object of interest only on the basis of its position in that CMD. We cleaned the YMCA-1's CMD using the photometry of a reference star field placed far from the object field, but not too far from it as to become unsuitable as representative of the star field projected along the line-of-sight (LOS) of YMCA-1. Even though YMCA-1 is located  $\sim 13^\circ$  to the East of the LMC centre, and therefore is not projected onto a crowded star field or is not affected by differential reddening, it is highly possible to find differences between the stellar density, magnitude and colour distributions of different adjacent

star fields surrounding YMCA-1. For this reason we decided to clean a circular area of radius  $0.5'$  centred on YMCA-1, using at a time six different circular areas with the same radius distributed around the YMCA-1's circle. We thus increase the statistics of the cleaning procedure.

The method employed to remove field stars was devised by [Piatti & Bica \(2012\)](#), which was satisfactorily applied elsewhere (e.g., [Piatti et al. 2018](#); [Piatti 2021b](#), and references therein). The procedure proved to be successful for clusters projected on to crowded fields and affected by differential reddening (see, e.g., [Piatti & Fernández-Trincado 2020](#), and references therein). It uses the magnitude and colour of each star in the reference star field CMD and finds the closest one in magnitude and colour in the YMCA's CMD and subtracts it. The methodology to select stars to subtract from the YMCA-1's CMD consists in defining boxes centred on the magnitude and colour of each star of the reference star field; then to superimpose them on to the YMCA's CMD, and finally to choose one star per box to subtract. We started with boxes with size of  $(\Delta g_0, \Delta(g-i)_0) = (1.00 \text{ mag}, 0.25 \text{ mag})$  centred on the  $(g_0, (g-i)_0)$  values of each reference field star, in order to guarantee to find a star in the YMCA's CMD with the magnitude and colour within the box boundary. The reddening corrected  $g_0, i_0$  magnitudes were derived by using the observed  $g, i$  magnitudes,  $E(B-V)$  values provided by SMASH and the  $A_\lambda/E(B-V)$  ratios, for  $\lambda = g, i$ , given by [Abbott et al. \(2018\)](#). In the case that more than one star is located inside a box, the closest one to the centre of that (magnitude, colour) box is subtracted. The magnitude and colour errors of the stars in the YMCA-1's CMD were taken into account while searching for a star to be subtracted. With that purpose, we allowed the search of stars in the YMCA-1's CMD to vary within an interval of  $\pm 1\sigma$ , where  $\sigma$  represents the errors in their magnitude and colour, respectively. We allowed up to 1000 random combination of their magnitude and colour errors.

The outcome of the cleaning procedure is a YMCA-1's CMD that likely contains only members. We finally assigned a membership probability to each star that remained unsubtracted after the decontamination of the YMCA-1's CMD. Because we produced six different cleaned CMDs (one per reference star field employed), we defined the probability  $P$  (%) =  $100 \times N/6$ , where  $N$  represents the number of times a star was not subtracted during the six different CMD cleaning executions. With that information on hand, we built Fig. 1, which shows the spatial distribution and the CMD of all the measured stars located in the field of YMCA-1. Stars with different  $P$  values were plotted with different colours. Fig. 1 reveals a red giant branch and a Main Sequence turnoff that are clearly highlighted as the most probable YMCA-1 sequences. From a total of 125 stars located in a circle of radius  $0.5'$ , 46 resulted with  $P > 50$  per cent.

We fitted theoretical isochrones computed by [Bressan et al. \(2012, PARSEC<sup>2</sup>\)](#) for the SMASH photometric system. We used PARSEC v1.2S isochrones spanning metallicities ( $\log(Z/Z_\odot)$ ) from 0.00005 dex up to 0.001 dex, in steps of 0.001 dex and  $\log(\text{age}/\text{yr})$  from 9.5 up to 10.1 in steps of 0.025. We fitted these isochrone sets to stars with  $P > 50$  per cent allowing the true distance modulus to vary between 18.0

<sup>1</sup> <https://datalab.noirlab.edu/smash/smash.php>

<sup>2</sup> <http://stev.oapd.inaf.it/cgi-bin/cmd>

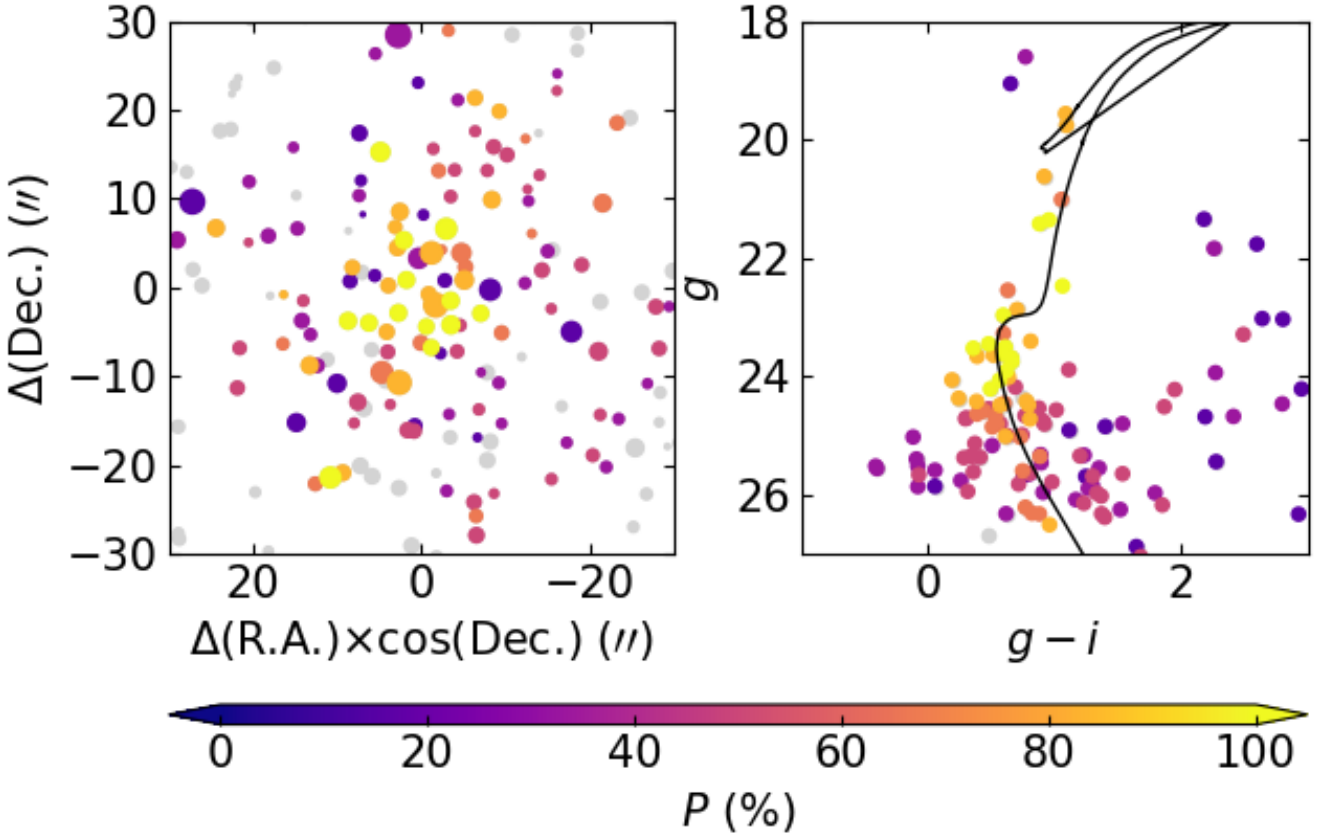


**Figure 1.** *Left panel:* Chart of all the measured stars in the field of YMCA-1. The size of the symbols is proportional to the  $g$  brightness of the star. *Right panel:* Colour-magnitude diagram of YMCA-1. The isochrone which best represents the distribution of stars with  $P > 50$  per cent is overlotted. Filled circles in both panels are colour-coded according to the assigned membership probability  $P$ .

mag (40 kpc) and 20.0 mag (100 kpc). We employed routines of the Automated Stellar Cluster Analysis code (ASteCA, Perren et al. 2015) that allowed us to derive simultaneously the metallicity, the age and the distance of YMCA-1. ASteCA is a suit of tools that produces a synthetic CMD that best matches the cleaned star cluster CMD. The metallicity, age, distance, reddening, star cluster present mass and binary fraction associated to that generated synthetic CMD were adopted as the best-fitted star cluster properties. Because individual  $E(B - V)$  values are available from the SMASH data sets, we entered into ASteCA with the intrinsic YMCA-1's CMD.

For generating the synthetic CMDs, we adopted the initial mass function of Kroupa (2002); a minimum mass ratio for the generation of binaries of 0.5. Star cluster mass and binary fractions were set in the ranges 100-5000  $M_{\odot}$  and 0.0-0.5, respectively. We explored the parameter space of the synthetic CMDs through the minimization of the likelihood function defined by Tremmel et al. (2013, the Poisson likelihood ratio (eq. 10)) using a parallel tempering Bayesian MCMC algorithm, and the optimal binning Knuth

(2018)'s method. Errors in the obtained parameters are estimated from the standard bootstrap method described in Efron (1982). We refer the reader to the work of Perren et al. (2015) for details concerning the implementation of these algorithms. The resulting fundamental parameters for YMCA-1 turned out to be: distance =  $60.9^{+14}_{-12}$  kpc (true distance modulus =  $18.92^{+0.45}_{-0.47}$  mag); age =  $9.6^{+3.5}_{-2.6}$  Gyr,  $[\text{Fe}/\text{H}] = -1.16^{+0.11}_{-0.14}$  dex; and present mass =  $435 \pm 157 M_{\odot}$ . The isochrone for the resulting mean values is superimposed in Fig. 1.

We also used stars with  $P > 50$  per cent to build the surface density profile of YMCA-1. In order to do that, we computed the integrated  $M_V$  magnitude in annuli of 0.02', 0.04', 0.06', 0.08' and 0.10' wide, and then calculated their average and dispersion. The integrated  $M_V$  magnitudes were computed from the sum of individual stellar luminosities ( $L_{\star}$ ), that were in turn obtained by interpolating the reddening free  $g_0$  magnitudes in the theoretical isochrone correspond-

ing to the mean age and metallicity of YMCA-1, and the following expression:

$$M_V = 4.72 - 2.5 \times \log(\sum L_*) + 0.18 \quad (1)$$

where 4.72 mag is the adopted bolometric magnitude of the Sun, and -0.18 mag is the mean bolometric correction from Masana et al. (2006, their figure 14) for a mean effective temperature of  $\log(T_{eff}) = 4.77 \pm 0.03$ , which corresponds to the average of individual effective temperatures interpolated in the above isochrone for stars with  $P > 50$  per cent. The resulting surface density profile with its respective uncertainties is depicted in Fig. 2, where we superimposed the best-fitted Plummer (1911)'s model (derived half-light radius  $r_h = 6.5^{+2.4}_{-2.5}$  arcsec, equivalent to  $1.92^{+0.72}_{-0.74}$  pc). As can be seen, the surface density profile is not smooth as those of populous globular clusters. This is because the number of stars is relatively small, and they are irregularly spatially distributed as a function of their brightnesses, so that stochastic effects have a role. Such stochastic effects are reflected in the  $r_h$  uncertainty. We also took advantage of the above equation to calculate the integrated  $M_V$  mag of YMCA-1, which turned out to be  $-1.70 \pm 0.50$  mag, where the uncertainty comes from using a Monte Carlo sampling of the involved parameters and their uncertainties.

Finally, from the *Gaia* Early Data Release<sup>3</sup> database (*Gaia* EDR3; Gaia Collaboration et al. 2016, 2020), we extracted parallaxes ( $\varpi$ ), proper motions in right ascension (pmra) and declination (pmdec), excess noise (epsi), the significance of excess of noise (sepsi), and  $G$ ,  $BP$ , and  $RP$  magnitudes for stars located within  $0.5'$  from the YMCA-1's centre. We pruned the data with  $sepsi < 2$  and  $epsi < 1$ , which define a good balance between data quality and the number of retained objects for our sample (see also Piatti 2021a, and references therein). We then built the vector point diagram, the CMD, and the parallax versus magnitude diagram (see Fig. 3) for all the retrieved stars. As can be seen, four stars drawn with red filled circles seem to be highly probable YMCA-1's members, because of their similar proper motions, of their placement along the red giant branch, and of their parallaxes. For them, we obtained  $\langle pmra \rangle = 1.044 \pm 0.402$  mas/yr and  $\langle pmdec \rangle = 1.107 \pm 0.209$  mas/yr. Table 1 summarizes the derived YMCA-1's properties.

### 3 ANALYSIS AND DISCUSSION

The brightness and size of YMCA-1 suggest that we are dealing with a small star cluster. Indeed, Fig. 4, top-left panel, shows that its integrated absolute magnitude  $M_V$  and projected half-light radius  $r_h$  are placed in the region of small MW open clusters, although it could also marginally belongs to the family of recently discovered faint old star clusters of the outer halo of the MW (see Fig. 4, top-right panel). Gatto et al. (2022) obtained a larger half-light radius (3.5 pc,  $\sim 2.2\sigma$  larger) and fainter absolute magnitude (-0.47 mag,  $\sim 2.5\sigma$  fainter) that make the object falls in the middle among these faint star clusters (Torrealba et al. 2019).

<sup>3</sup> <https://archives.esac.esa.int/gaia>.

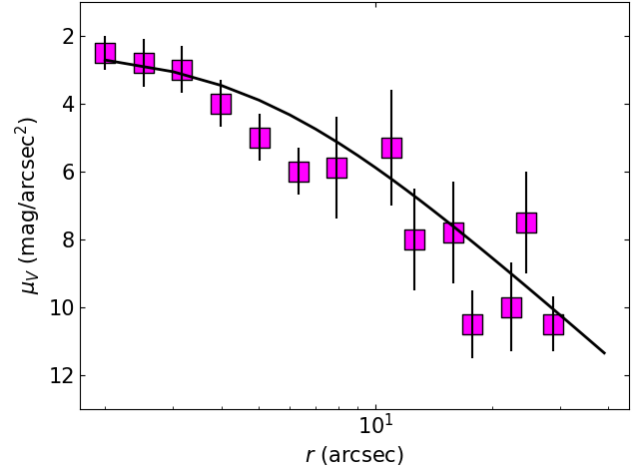


**Figure 2.** Surface density profile built from stars with membership probability  $P > 50$  per cent. The best-fitted Plummer (1911)'s model ( $r_h = 6.5$  arcsec, equivalent to 1.92 pc) is overplotted.

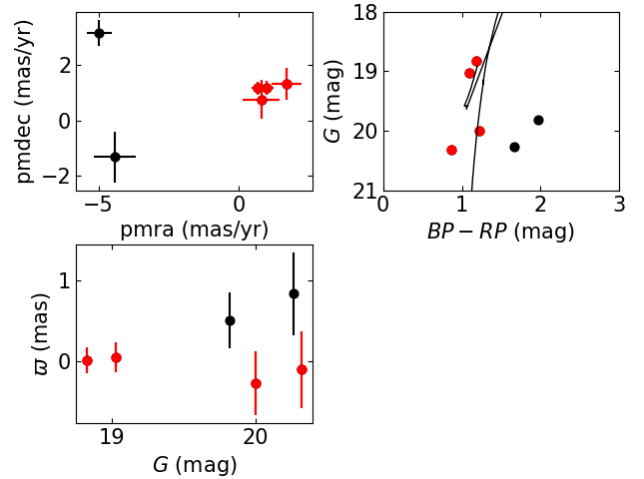


**Figure 3.** Relationships between *Gaia* EDR3 retrieved parameters for stars located within a circle of radius  $0.5'$  from the YMCA-1's centre. We represented highly probable members with filled circles. The theoretical isochrone for the adopted mean distance, age, and metallicity is overplotted in the *Gaia* CMD.

Although there are very few MW open clusters with an age similar to that of YMCA-1 (Anders et al. 2021), none of them is as metal deficient as  $[Fe/H] \sim -1.2$  dex; the most metal-poor open clusters having  $[Fe/H] \sim -0.5$  dex (Dias et al. 2021). This implies that YMCA-1 departs significantly from the age-metallicity relationship of the MW disk, and hence we conclude that it could not have formed in the Milky Way. YMCA-1 would not seem to be part of the population of MW globular clusters formed in-situ either, because of its distinct age and metallicity (see upper sequence of black filled circles in Fig. 4, bottom panel (Kruijssen et al. 2019)). Globular clusters associated with dwarf galaxy accretion events (e.g., Sagittarius, Gaia-Enceladus, Sequoia, Koala, etc), are distributed along the lower sequence of black filled circles of Fig. 4, bottom panel. YMCA-

**Table 1.** Derived properties of YMCA-1

Property	value
$\alpha_{2000}$	110.8378 $^{\circ}$
$\delta_{2000}$	-64.8319 $^{\circ}$
$r_h$	1.92 $^{+0.72}_{-0.74}$ pc
$(m - M)_0$	18.92 $^{+0.45}_{-0.47}$ mag
distance <sub>MW</sub>	60.9 $^{+14}_{-12}$ kpc
distance <sub>LMC</sub>	$\sim 17.1$ kpc
distance <sub>SMC</sub>	$\sim 86.0$ kpc
Age	9.6 $^{+3.5}_{-2.6}$ Gyr
[Fe/H]	-1.16 $^{+0.11}_{-0.14}$ dex
Mass	435 $\pm 157$ $M_{\odot}$
$\langle \log(T_{eff}) \rangle$	4.77 $\pm 0.03$
$M_V$	-1.70 $\pm 0.50$ mag
$\langle \text{pmra} \rangle$	1.044 $\pm 0.402$ mas/yr
$\langle \text{pmdec} \rangle$	1.107 $\pm 0.209$ mas/yr

1 falls slightly below it, while according to Forbes (2020), the age-metallicity relationship of the High-Energy group of globular clusters would seem to be the closest to the YMCA-1 placement. These distant globular clusters spend much of their lifetime in the outer MW halo, so that they have experienced less severe mass loss due to tidal effects than those in the inner Galactic regions (Piatti 2019; Piatti et al. 2019b). Their present masses are a couple of orders of magnitude larger than YMCA-1’s derived mass, making it unlikely that YMCA-1 is a member of this outer globular cluster population, although the age-metallicity relationship shows some overlap when the age error is considered.

The similitude of YMCA-1 with the recently discovered faint old star clusters is much difficult to disentangle. Indeed, some of them follow the age-metallicity relationship sequence of accreted globular clusters (from the oldest ages until  $\sim 6$  Gyrs ago; see Fig. 4, bottom panel), while others are metal-poor star clusters ( $[\text{Fe}/\text{H}] \lesssim -1.4$  dex) and as old as YMCA-1. None of these two sequences of old clusters would clearly seem to be that which YMCA-1 belongs to. As can be seen in Fig. 4, bottom panel, YMCA-1 is in between them. Nonetheless, because of the age uncertainty of YMCA-1, the above scenarios should not be ruled out as possible origin of YMCA-1.

Having examined the possibility of YMCA-1 to be a MW star cluster, formed in-situ or ex-situ, we analyse now whether it could have been born in the Magellanic Clouds. The LMC is known to harbour a population of  $\sim 15$  globular clusters older than  $\sim 12$  Gyr and with metallicities more deficient than  $[\text{Fe}/\text{H}] \sim -1.3$  dex (Piatti et al. 2019a). The absence of star clusters with ages between  $\sim 4$  and 11 Gyr, with the sole exception of ESO 121-SC03 and KMHK 1592 (Piatti 2022), have been extensively reported in the literature (see Fig 4, bottom panel). In the SMC there are some five star clusters with ages between  $\sim 7$  and 12 Gyr and metallicities in the range  $-1.2 \lesssim [\text{Fe}/\text{H}]$  (dex)  $\lesssim -1.0$  (Piatti 2011, see also Fig. 4 here). Star clusters and field stars in the LMC and the SMC have similar age-metallicity relationships (Narloch et al. 2021; Piatti 2021c), so that we would expect star clusters formed at any age accompanying the field star formation, which has not been interrupted in both galaxies since their formation (Piatti & Geisler 2013; Mazzi et al. 2021). This is not the case of LMC star cluster popu-

lation, where we note the existence of only two star clusters of 8-9 Gyr old in the so-called LMC age gap (Piatti 2022). For this reason, we think that an SMC origin could explain the appearance of YMCA-1 in the outskirts of the LMC, at a distance of  $\sim 17.1$  kpc from its centre, unless an enough large population of 4-11 Gyr old clusters is discovered in the LMC.

Recently, Gatto et al. (2022) obtained deep VLT photometry with the aim of disentangling the nature of YMCA-1 and determining its fundamental parameters. Because of their resulting distance (55.5 kpc), they concluded that the object is associated to the LMC, although a MW satellite is not discarded either. According to them, YMCA-1 is placed in a transition region of the  $M_V$  versus  $r_h$  plane, between ultra-faint dwarf galaxies and open clusters. They estimated an  $r_h$  of 3.5 pc from the fit of a smooth stellar number density profile (see their Figure 1, right panel). We note that a circle of radius 3.5 pc (12.9 $''$ ) nearly encompasses the entire cluster main body (see their Fig. 1, middle panel). For these reasons we adopted our present  $r_h$  value, which supports the existence of a small star cluster. On the other hand, Gatto et al. (2022) used as priors for determining the cluster astrophysical parameters ages larger than 10 Gyr and distances smaller than the value derived in Gatto et al. (2021), which constrained the fitting procedure. We used wider ranges of ages and distances as ASteCA’s inputs and obtained parameters in an overall agreement with those of Gatto et al. (2022) and larger uncertainties. We think that the latter are more realistic.

The tidal interaction between both Magellanic Clouds (Wan et al. 2020; Ruiz-Lara et al. 2020; Mazzi et al. 2021; Williams et al. 2021; Roman-Duval et al. 2021; Grady et al. 2021; Shipp et al. 2021; Cullinane et al. 2022, among others) can also be a source for star clusters formed in the SMC were then stripped off by the LMC. Such a scenario was explored numerically by Carpintero et al. (2013), who modelled the dynamical interaction between both galaxies and their corresponding stellar cluster populations. They found that nearly 15 per cent of the SMC star clusters are captured by the LMC with eccentricities of the orbit of the SMC around the LMC  $\gtrsim 0.4$ , while another 20-50 per cent is scattered into the intergalactic environment. Consequently, star clusters that originally belonged to the SMC could more likely be found in the outskirts of the LMC. YMCA-1 could form in the SMC (its age and metallicity agree well with the older enhanced formation event in the SMC (Piatti 2011, 2012) and later captured by the LMC.

In order to confirm such a hypothesis, we have integrated the orbit of YMCA-1 backwards in time with respect to the MW-LMC-SMC system. The galaxies were included as point particles representing their gaseous and stellar disks with radially extended dark matter (DM) halos following Hernquist profiles (Hernquist 1990) including the effects of dynamical friction. The MW was included as a live particle (not a static potential) thus allowing for the impact of its reflex motion on the other galaxies’ orbits (Gómez et al. 2015). The properties of these galaxies are listed in Table 2.

We used the RA, Dec, distance, and proper motions of YMCA-1 to obtain 3D Galactocentric cylindrical coordinates using Astropy (Astropy Collaboration et al. 2013, 2018) assuming a radial velocity (RV) ranging from 0 to 500 km/s. The orbits of the Magellanic Clouds around the MW

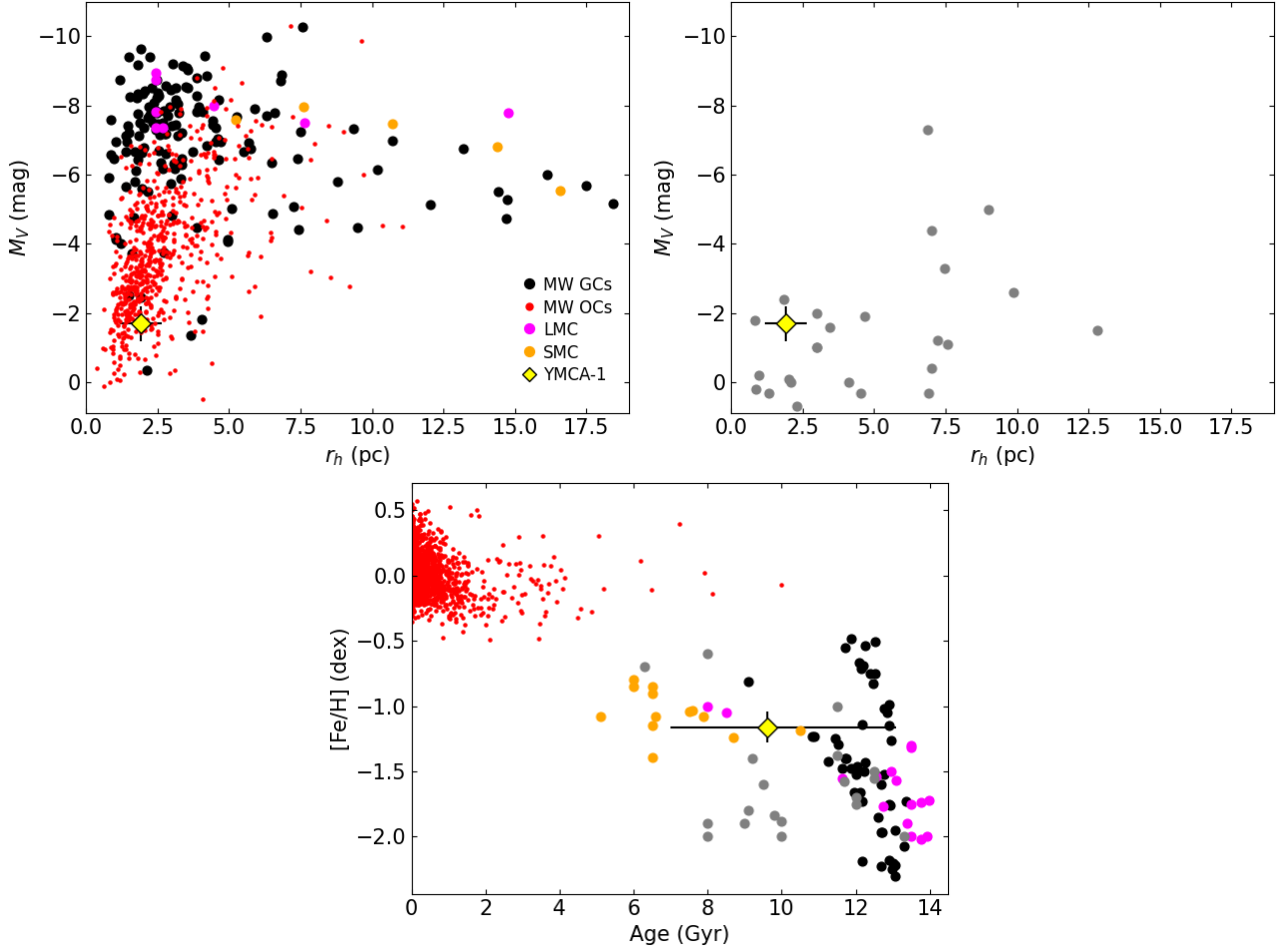


**Figure 4.** *Left-top panel:*  $M_V$  versus  $r_h$  relationship for MW globular clusters (black filled circles; Harris 1996; Kruijssen et al. 2019); LMC and SMC globular clusters (magenta and orange filled circles, respectively; Glatt et al. 2009; Mackey & Gilmore 2003; Baumgardt et al. 2013; Piatti & Mackey 2018; Piatti et al. 2019a; Song et al. 2021; Parisi et al. 2022); and MW open clusters (red points; Kharchenko et al. 2009, 2013; Dias et al. 2021). YMCA-1 is represented by a large filled yellow diamond, with its respective error bars. *Right-top panel:* same as left panel for recently discovered faint star clusters in the MW halo: Balbinot 1 (Balbinot et al. 2013), BLISS 1 (Mau et al. 2019), DELVE 1 (Mau et al. 2020), DELVE 2 (Cerny et al. 2021), DES 1 (Luque et al. 2016), DESJ0111-1341 (Luque et al. 2017), DES 3 (Luque et al. 2018), DES 4 and 5 (Torrealba et al. 2019), Gaia 1 y 2 (Koposov et al. 2017), Gaia 3 to 7 (Torrealba et al. 2019), Kim 1 (Kim & Jerjen 2015), Kim 2 (Kim et al. 2015), Kim 3 (Kim et al. 2016), Koposov 1 and 2 (Koposov et al. 2007), Laevens 3 (Laevens et al. 2015), Muñoz 1 (Muñoz et al. 2012), PSOJ174.0675-10.8774 (Laevens et al. 2014), PS1 1 (Torrealba et al. 2019), Segue 3 (Fadely et al. 2011), and To 1 (Torrealba et al. 2019). *Bottom panel:* age-metallicity relationship. Symbols and references as in the top panels.

with the various possible orbits of YMCA-1 are shown in Fig. 5. Note that these orbits are being evolved backwards in time, so a positive RV (the cluster moving away from us at the present day) corresponds to the cluster moving closer to us in its recent past. For RVs greater than the LMC’s observed value of  $262.2 \text{ km s}^{-1}$  (van der Marel et al. 2002) the cluster is bound to the LMC and completes 2-3 orbits around it within the past 500 Myrs. This is the case even when integrating the orbits back 3 Gyr: YMCA-1 remains bound to the LMC if its RV  $\gtrsim 300 \text{ km s}^{-1}$ .

In addition to testing different RVs for the cluster, we also explored possible orbits within the uncertainties of the velocities of the LMC and SMC, as well as the uncertainties in the distance and proper motions of YMCA-1. For these integrations we took a fiducial value for the RV of  $400 \text{ km s}^{-1}$ . We used a Monte Carlo method to sample a set of velocities for the Magellanic Clouds within the range of their

observed errors (listed in Table 2). We took 1,000 samples and YMCA-1 remains bound to the LMC in all cases. There are 8 integrations (0.8 per cent) in which the cluster eventually escapes the LMC, however this is only after at least 3 orbits.

We also performed Monte Carlo simulations with respect to the distance and proper motion errors of YMCA-1. From the 1,000 samples taken, 587 integrations (58.7 per cent) result in YMCA-1 being bound to the LMC for at least 2 orbits and approaching a distance  $< 10 \text{ kpc}$ . The separation between the LMC and YMCA-1 as a function of time is shown in Fig. 6 for a subset of this parameter space. 27 integrations are shown corresponding to all combinations of +1, 0, and -1 sigma in distance, pmra, and pmdec. The lines in this figure are coloured by the minimum separation between the LMC and YMCA-1 over the past 500 Myr and the fiducial case (0 sigma for all three parameters) is shown

as a bold line. For larger present-day distances or smaller pmra, the cluster doesn't approach the LMC as closely and therefore is less likely to have been bound to the LMC.

#### 4 CONCLUSIONS

We used SMASH and *Gaia* EDR3 data to determine the astrophysical parameters of YMCA-1, a stellar object recently discovered in the outskirts of the LMC. While [Gatto et al. \(2021\)](#) suggested that it is a halo star cluster located at 100 kpc from the Galactic centre, [Gatto et al. \(2022\)](#) confirmed its closer distance, at 55 kpc from the Sun, although they were inconclusive about its physical nature. The object caught our attention because of the possibility of being a witness of the interaction between both Magellanic Clouds.

SMASH data of stars in the YMCA-1 field, once they were properly treated in order to disentangle member from field stars, revealed the existence of a small star cluster as assessed from the derived integrated  $M_V$  magnitude and half-light radius using stars with membership probabilities  $> 50$  per cent. Its CMD was used to derive its fundamental properties by exploring the parameter space using synthetic CMDs through the minimization of likelihood functions and obtained parameters uncertainties from standard bootstrap methods. YMCA-1 turned out to be a small ( $435 M_\odot$ ) moderately old (age = 9.6 Gyr), moderately metal-poor ( $[\text{Fe}/\text{H}] = -1.16$  dex) star cluster, located at a nearly SMC distance (60.9 kpc) from the Sun, at  $\sim 17.1$  kpc to the East from the LMC centre. *Gaia* EDR3 data of four likely red giant members allowed us to derive the mean cluster proper motions. The brightness and size of YMCA-1 suggest some resemblance to the recently discovered faint star clusters in the MW outer halo, although YMCA-1 would not seem to match their age-metallicity relationship, nor those of MW globular clusters formed in-situ or ex-situ, besides the fact that YMCA-1 is some order of magnitudes less massive than distant halo globular clusters. We also dismissed an LMC origin, because the cluster age falls within the well-known LMC cluster age gap, and its metallicity is marginally consistent with the LMC age-metallicity relationship. Conversely, the entire set of derived parameters of YMCA-1 tightly match those of SMC star clusters and field stars.

We performed extensive numerical Monte Carlo simulations in order to trace its trajectory in the space backward in time. By considering the MW, the LMC, and the SMC discs as dynamic point particles embedded in radially extended dark matter haloes that experience dynamical friction, we explored different RV regimes for YMCA-1 finding that RVs  $\gtrsim 300$  km/s lead to bound orbits around the LMC during the past 500 Myrs. Such an orbital configuration is confirmed when uncertainties in the velocities of the LMC and SMC, as well as those in the distance and proper motions of YMCA-1 are included. The resulting orbital motions would seem to suggest that YMCA-1 would not be bound to nor would have been born in the MW, and its apparent mismatch with the LMC cluster population properties would lead to speculate on an SMC origin. Such a scenario was predicted by [Carpintero et al. \(2013\)](#), making YMCA-1 the first tracked star cluster that could have been stripped by the LMC during any of its approaching to the SMC.

#### ACKNOWLEDGEMENTS

We thank the referee for the thorough reading of the manuscript and timely suggestions to improve it.

#### 5 DATA AVAILABILITY

Data used in this work are available upon request to the authors.

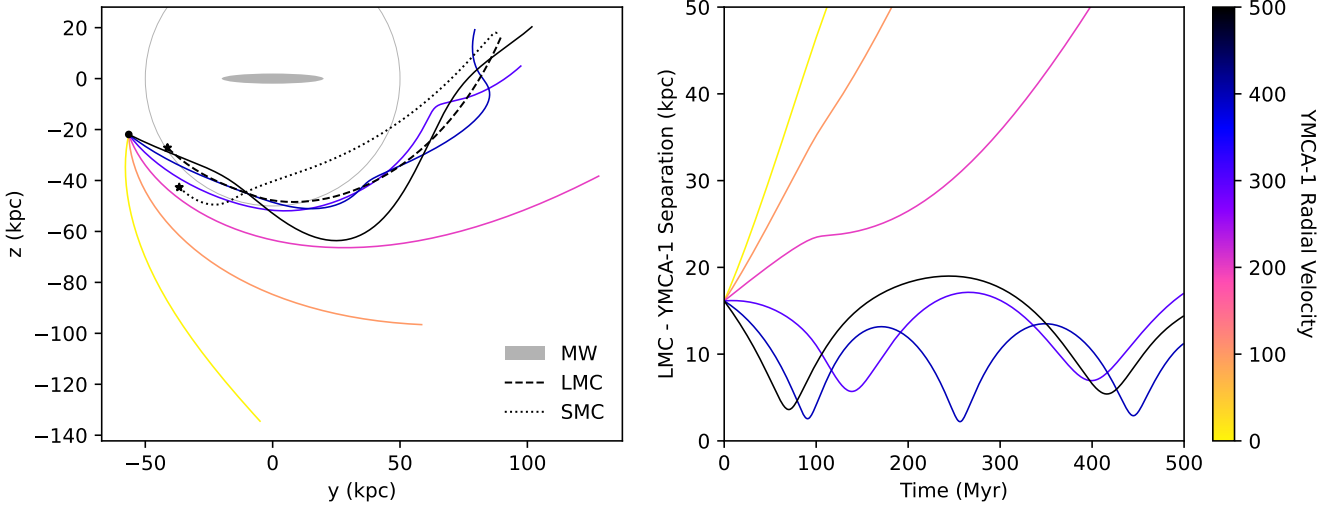


**Figure 5.** Orbits of YMCA-1. The left panel shows the projection of the orbits of the LMC (dashed black line), SMC (dotted black line), and YMCA-1 (lines coloured by present-day RV) around the MW (grey oval) over the past 500 Myrs in the  $y$ - $z$  plane. In this coordinate system, the disk of the MW is assumed to be in the  $x$ - $y$  plane with the Sun's position at  $(x, y, z) = (-8.1, 0, 0.02)$  kpc. The grey circle denotes 50 kpc away from the MW.

**Table 2.** Adopted parameter for the MW, LMC, and SMC, respectively.

	MW	LMC	SMC
DM Mass ( $M_{\odot}$ )	$10^{12}$	$1.8 \times 10^{11}$	$1.9 \times 10^{10}$
$r_{200}$ (kpc)	166.1	92.72	45.22
Hernquist Scale Length (kpc)	8.6	4.6	2.2
Disk Mass <sup>a</sup> ( $M_{\odot}$ )	$5.8 \times 10^{10}$	$10^{10}$	$2 \times 10^9$
Present-day Position <sup>b</sup> (kpc)	—	(-0.76, -41.29, -27.15)	(15.20, -36.68, -42.67)
Present-day Velocity <sup>b</sup> ( $\text{km s}^{-1}$ )	—	$(-57 \pm 13, -226 \pm 15, 221 \pm 19)^c$	$(18 \pm 6, -179 \pm 16, 174 \pm 13)^d$

<sup>a</sup> Including both the stellar and gaseous components.

<sup>b</sup> In Cartesian coordinates  $(x, y, z)$  centered on the MW with the sun located at  $(x, y, z) = (-8.1, 0, 0.02)$  kpc.

<sup>c</sup> Kallivayalil et al. (2013); <sup>d</sup> Zivick et al. (2018).

## REFERENCES

- Abbott T. M. C., et al., 2018, *ApJS*, **239**, 18
- Anders F., Cantat-Gaudin T., Quadrino-Lodoso I., Gieles M., Jordi C., Castro-Ginard A., Balaguer-Núñez L., 2021, *A&A*, **645**, L2
- Astropy Collaboration et al., 2013, *A&A*, **558**, A33
- Astropy Collaboration et al., 2018, *AJ*, **156**, 123
- Balbinot E., et al., 2013, *ApJ*, **767**, 101
- Baumgardt H., Parmentier G., Anders P., Grebel E. K., 2013, *MNRAS*, **430**, 676
- Bica E., Westera P., Kerber L. d. O., Dias B., Maia F., Santos João F. C. J., Barbuy B., Oliveira R. A. P., 2020, *AJ*, **159**, 82
- Bressan A., Marigo P., Girardi L., Salasnich B., Dal Cero C., Rubele S., Nanni A., 2012, *MNRAS*, **427**, 127
- Carpintero D. D., Gómez F. A., Piatti A. E., 2013, *MNRAS*, **435**, L63
- Cerny W., et al., 2021, *ApJ*, **910**, 18
- Cullinane L. R., Mackey A. D., Da Costa G. S., Erkal D., Koposov S. E., Belokurov V., 2022, *MNRAS*, **510**, 445
- Dias W. S., Monteiro H., Moitinho A., Lépine J. R. D., Carraro G., Paunzen E., Alessi B., Vilella L., 2021, *MNRAS*, **504**, 356
- Drlica-Wagner A., et al., 2021, *ApJS*, **256**, 2
- Efron B., 1982, The Jackknife, the Bootstrap and other resampling plans
- Fadely R., Willman B., Geha M., Walsh S., Muñoz R. R., Jerjen H., Vargas L. C., Da Costa G. S., 2011, *AJ*, **142**, 88
- Forbes D. A., 2020, *MNRAS*, **493**, 847
- Gaia Collaboration et al., 2016, *A&A*, **595**, A1
- Gaia Collaboration et al., 2020, arXiv e-prints, p. arXiv:2012.01771
- Gatto M., et al., 2021, *Research Notes of the American Astronomical Society*, **5**, 159
- Gatto M., et al., 2022, arXiv e-prints, p. arXiv:2204.02420
- Geisler D., Bica E., Dottori H., Claria J. J., Piatti A. E., Santos Jr. J. F. C., 1997, *AJ*, **114**, 1920
- Glatt K., et al., 2009, *AJ*, **138**, 1403
- Gómez F. A., Besla G., Carpintero D. D., Villalobos Á., O'Shea B. W., Bell E. F., 2015, *ApJ*, **802**, 128
- Grady J., Belokurov V., Evans N. W., 2021, *ApJ*, **909**, 150
- Harris W. E., 1996, *AJ*, **112**, 1487
- Hernquist L., 1990, *ApJ*, **356**, 359
- Kallivayalil N., van der Marel R. P., Besla G., Anderson J., Alcock C., 2013, *ApJ*, **764**, 161
- Kharchenko N. V., Piskunov A. E., Röser S., Schilbach E., Scholz R. D., Zinnecker H., 2009, *A&A*, **504**, 681
- Kharchenko N. V., Piskunov A. E., Schilbach E., Röser S., Scholz R. D., 2013, *A&A*, **558**, A53
- Kim D., Jerjen H., 2015, *ApJ*, **799**, 73
- Kim D., Jerjen H., Milone A. P., Mackey D., Da Costa G. S.,



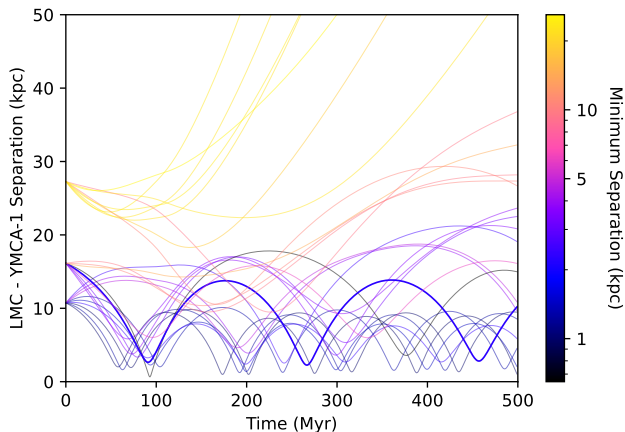


**Figure 6.** Impact of YMCA-1 uncertainties on its orbit. The separation between the LMC and YMCA-1 as a function of time for the 27 integrations in which the cluster's distance and proper motions are shifted by  $-1$ ,  $0$ , and  $+1$  sigma is shown. The lines are coloured by the minimum approach of the cluster to the LMC within the past 500 Myrs. The fiducial orbit is shown in bold (corresponding to distance = 60.9 kpc, pmra = 1.044 mas yr $^{-1}$ , and pmdec = 1.107 mas yr $^{-1}$ ).

2015, *ApJ*, 803, 63  
 Kim D., Jerjen H., Mackey D., Da Costa G. S., Milone A. P., 2016, *ApJ*, 820, 119  
 Knuth K. H., 2018, optBINS: Optimal Binning for histograms (ascl:1803.013)  
 Koposov S., et al., 2007, *ApJ*, 669, 337  
 Koposov S. E., Belokurov V., Torrealba G., 2017, *MNRAS*, 470, 2702  
 Kroupa P., 2002, *Science*, 295, 82  
 Kruijssen J. M. D., Pfeffer J. L., Reina-Campos M., Crain R. A., Bastian N., 2019, *MNRAS*, 486, 3180  
 Laevens B. P. M., et al., 2014, *ApJ*, 786, L3  
 Laevens B. P. M., et al., 2015, *ApJ*, 813, 44  
 Luque E., et al., 2016, *MNRAS*, 458, 603  
 Luque E., et al., 2017, *MNRAS*, 468, 97  
 Luque E., et al., 2018, *MNRAS*, 478, 2006  
 Mackey A. D., Gilmore G. F., 2003, *MNRAS*, 338, 120  
 Martin N. F., et al., 2016, *ApJ*, 830, L10  
 Masana E., Jordi C., Ribas I., 2006, *A&A*, 450, 735  
 Mau S., et al., 2019, *ApJ*, 875, 154  
 Mau S., et al., 2020, *ApJ*, 890, 136  
 Mazzi A., et al., 2021, *MNRAS*, 508, 245  
 Muñoz R. R., Geha M., Côté P., Vargas L. C., Santana F. A., Stetson P., Simon J. D., Djorgovski S. G., 2012, *ApJ*, 753, L15  
 Narloch W., et al., 2021, *A&A*, 647, A135  
 Nidever D. L., et al., 2017, *AJ*, 154, 199  
 Nidever D. L., et al., 2021, *AJ*, 161, 74  
 Parisi M. C., Gramajo L. V., Geisler D., Dias B., Clariá J. J., Da Costa G., Grebel E. K., 2022, arXiv e-prints, p. arXiv:2203.06542  
 Perren G. I., Vázquez R. A., Piatti A. E., 2015, *A&A*, 576, A6  
 Piatti A. E., 2011, *MNRAS*, 418, L69  
 Piatti A. E., 2012, *MNRAS*, 422, 1109  
 Piatti A. E., 2019, *ApJ*, 882, 98  
 Piatti A. E., 2021a, arXiv e-prints, p. arXiv:2104.03750  
 Piatti A. E., 2021b, *AJ*, 161, 199  
 Piatti A. E., 2021c, *A&A*, 647, A47  
 Piatti A. E., 2022, *MNRAS*, 511, L72

Piatti A. E., Bica E., 2012, *MNRAS*, 425, 3085  
 Piatti A. E., Fernández-Trincado J. G., 2020, *A&A*, 635, A93  
 Piatti A. E., Geisler D., 2013, *AJ*, 145, 17  
 Piatti A. E., Mackey A. D., 2018, *MNRAS*, 478, 2164  
 Piatti A. E., Cole A. A., Emptage B., 2018, *MNRAS*, 473, 105  
 Piatti A. E., Alfaro E. J., Cantat-Gaudin T., 2019a, *MNRAS*, 484, L19  
 Piatti A. E., Webb J. J., Carlberg R. G., 2019b, *MNRAS*, 489, 4367  
 Plummer H. C., 1911, *MNRAS*, 71, 460  
 Roman-Duval J., et al., 2021, *ApJ*, 910, 95  
 Ruiz-Lara T., et al., 2020, *A&A*, 639, L3  
 Shipp N., et al., 2021, *ApJ*, 923, 149  
 Song Y.-Y., Mateo M., Bailey John I. I., Walker M. G., Roederer I. U., Olszewski E. W., Reiter M., Kremin A., 2021, *MNRAS*, 504, 4160  
 Torrealba G., Belokurov V., Koposov S. E., 2019, *MNRAS*, 484, 2181  
 Tremmel M., et al., 2013, *ApJ*, 766, 19  
 van der Marel R. P., Alves D. R., Hardy E., Suntzeff N. B., 2002, *AJ*, 124, 2639  
 Wan Z., Guglielmo M., Lewis G. F., Mackey D., Ibata R. A., 2020, *MNRAS*, 492, 782  
 Williams M. L., Bekki K., McKenzie M., 2021, *MNRAS*,  
 Zivick P., et al., 2018, *ApJ*, 864, 55

This paper has been typeset from a  $\text{\TeX}/\text{\LaTeX}$  file prepared by the author.